Supporting Information

Highly fluorescent conjugated microporous polymers for concurrent adsorption and detection of uranium

*Meiyun Xu, Tao Wang, Peng Gao, Li Zhao, Lei Zhou, Daoben Hua**

[a] State Key Laboratory of Radiation Medicine and Protection, School of Radiological and Interdisciplinary Sciences (RAD-X), Soochow University, Suzhou 215123, China.

[b] Collaborative Innovation Center of Radiological Medicine of Jiangsu Higher Education Institutions, Suzhou 215123, China.

*Corresponding author. Email: dbhua_lab@suda.edu.cn (D. Hua); Tel & Fax: +86-512-65883261.

Table of contents

1. Materials and characterization

1,3,5-Triethynylbenzene (J&K Chemical Technology Co., Ltd.), 2,7-dibromo-9H-fluorene (BePharm Ltd), tetrakis (triphenylphosphine)-palladium(0) [$Pd(PPh_3)_4$], CuI and acrylonitrile (Sinopharm Chemical Reagent Co., Ltd.), hydroxylamine hydrochloride (CP, Shanghai Macklin Biochemical Co., Ltd), and uranyl nitrate $UO_2(NO_3)_2 \cdot 6H_2O$ (Fluka, AR) were used as received. DMF was dried over CaH_2 and distilled prior to use. Triethylamine was dried over 4Å molecular sieve. All other solvents used in the experiments were of analytical grade. Ultrapure water used in the all experiments was obtained from Milli-Q water purification system (Milli-pore Corporation, USA).

Transmission electron microscopy (TEM) was performed on a Tecnai G2 spirit BioTwin field emission scanning electron microscope. X-ray photoelectron spectroscopy (XPS) was carried out by an ESCALAB 250Xi spectrometer. Fourier transform infrared (FTIR) spectra were recorded on a Varian-1000 spectrometer. Solid-state ^{13}C CP/MAS NMR measurements were carried out on a Bruker Avance III model 400 MHz NMR spectrometer at a MAS rate of 5 kHz. Surface areas and pore size distributions were measured by N_2 sorption and desorption at 77.3 K using the ASAP 2020 volumetric sorption analyzer. BET surface areas were calculated over the relative pressure range 0.05-0.15 P/P_0. Samples were degassed at 100 °C for 10 h under high vacuum before analysis. The concentration of uranium (VI) was determined by thermo high-resolution inductively coupled plasma mass spectrometry (ICP-MS, Element II).

2. Synthesis of 3,3'-(2,7-dibromo-9H-fluorene-9,9-diyl)dipropanenitrile (FCN).

A suspension of 2,7-dibromo-9H-fluorene (2.00 g, 6.16 mmol) and benzyltriethyl- ammonium chloride (8.75 mg, 0.04 mmol) in dioxane (15 g) was degassed and backfilled with nitrogen gas three times. 15% NaOH (0.3 g) and acrylonitrile (0.75g, 14.20 mmol) were added dropwise *via* a syringe successively, and the content was stirred under N_2 for 30 min at room temperature. 80 mL heptane was added into the resulting mixture. The solid was filtered, washed three times with heptane and methanol, and then dried at 50 ^oC *in vacuo* to give FCN as a white powder in 90% yield. ^1H NMR ($CDCl_3$, 400 MHz), δ 7.59 (4H, m), 7.51 (2H, m), 2.43 (4H, t, *J*=5.2 Hz), 1.57 (4H, q, *J* = 5.2 Hz).

3. Synthesis of CMPH.

CMPH was synthesized according to reported literature.[1-2] Nitrogen was bubbled to the DMF solution (8 mL) of 1,3,5-Triethynylbenzene (100 mg, 0.666 mmol) and F (215.7 mg, 0.666 mmol)

for 30 min. $Pd(PPh_3)_4$ (23.1 mg, 0.02 mmol) and CuI (7.6 mg, 0.04 mmol) were added into the solution followed by injection of 8 mL Et_3N. The reaction mixture was stirred at 90°C under N_2 for 48 hours. After cooling down, the mixture was filtered, and then washed with hot DMF for 2 times. The residue was dispersed in 100 mL THF with sonication, and then stirred with refluxed THF under N_2 for 2 hours. After cooling down, the mixture was filtered, and the proceed was repeated for 3 times. The coarse product was further washed with hot methanol for 48 hours by Soxhlet extraction, and then dried under vacuum at 50 °C to give CMPH (200 mg) in 96% yield as a yellow powder.

4. Theory and Calculation.

4.1 BET calculation

BET equations can be described as follows:

$$\frac{1}{V(p_0/p - 1)} = \frac{C-1}{V_m C} \times \frac{p}{p_0} + \frac{1}{V_m C} \quad (1)$$

$$S = \frac{V_m}{22400} N_A \sigma_m \times 10^{-18} \quad (2)$$

where V is sorption capacity (cc/g), p/p_0 is the relative pressure, constant V_m (cc/g) stands for the adsorption capacity of solid surface covered with molecular layer cc/g, C is a constant relating to adsorption heat, S is the total specific surface area of adsorbent, σ_m is the cross section area of adsorbate molecule (nm^2), and N_A is Avogadro constant. Constant V_m and C can be determined from the plot of $1/(V(p_0/p-1))$ against p_0/p (Table S6 and Figure S7).

4.2 Sorption kinetics[3-4]

Pseudo-first-order equation is described as following Equation (3):

$$\log(q_e - q_t) = \log q_e - (\frac{k_1}{2.303}) \times t \quad (3)$$

where q_e and q_t (mg g^{-1}) are the sorption capacity of U(VI) at equilibrium time and contact time t [min], respectively, and k_1 [min^{-1}] represents the pseudo first order kinetic constant. q_e and k_1 can be calculated from the slope and intercept of the plot of log (q_e-q_t) versus t, respectively (Figure S10A).

Pseudo-second-order model is expressed as the following Equation (4):

$$\frac{t}{q_t} = \frac{1}{k_2 \times q_e^2} + \frac{t}{q_e} \quad (4)$$

where k_2 [g/mg/min] represents the rate constant of the pseudo-second order model, and can be

determined from the plot of t/q_t against t (Figure S10B).

4.3 Sorption isotherms[5]

Langmuir model can be described as Equation (5):

$$\frac{C_e}{q_e} = \frac{1}{q_{\max} b} + \frac{C_e}{q_{\max}} \quad (5)$$

where b [L mg^{-1}] is the Langmuir constant related to the affinity of binding sites, and q_{max} [mg g^{-1}] is the maximum sorption capacity. They can be calculated from the linear plot of C_e/q_e against C_e (Figure S12A).

The Freundlich model[1] is applied for multilayer sorption, which can be described as Equation (6):

$$\log q_e = \log K_F + \frac{1}{n} \log C_e \quad (6)$$

where K_F [mg/g (L/mg)$^{1/n}$] and n are the Freundlich constants related to sorption capacity and sorption intensity, respectively, which can be calculated from the linear plot of log q_e versus log C_e (Figure S12B).

4.4 Selectivity coefficients for uranium (VI) (S_U)[6]

The selectivity coefficients for uranium (VI) (S_U) can be calculated according to Equation (7):

$$S_U = \frac{q_{e,U}}{q_{e,total}} \times 100\% \quad (7)$$

where $q_{e,U}$ and $q_{e,total}$ (mmol/g) are the sorption capacity for uranium (VI) and the competing metal ions, respectively.

4.5 Detection limit (DT) in deionized water.[7]

Based on the fluorescence measurement shown in Figure 6, the linear correlation in low uranyl concentration range (Figure S18) can be fitted as

y=105.79x+1.06 (8)

where y is the relative decrease of luminescence intensity ((I_0-I)/I_0)% monitored at 483 nm, and x is the uranyl concentration.

The standard deviation (σ) is defined as 100 × (I_{SE}/I_0), where I_{SE} is the standard error of the emission measurement, as determined by the baseline measurement of blank samples (monitored at 483 nm), I_0 is the luminescence intensity of CMPAO-4 in deionized water (also monitored at 483 nm).

The detection limit is calculated according to Equation (9) and (10):

$$DT = {}^{3\sigma}\!/_{slope} \quad (9)$$

$$\sigma = 100 \times ({}^{I_{SE}}\!/_{I_0}) \quad (10)$$

If defining three times of the standard deviation as the detectable signal, the detection limit can be projected as $3\sigma/slope = 0.4$ μg/L (1.7×10^{-9} M).

Table S1. The content of Pd and Cu in the materials from XPS progressive etching.

Sorbent	Pd (% atomic)*	Cu (% atomic)*
CMPH	0.29	0.47
CMPCN	0.34	0.58
CMPAO-1	0.24	0.63
CMPAO-2	0.22	0.48
CMPAO-3	0.25	0.60
CMPAO-4	0.20	0.51

*: the average value of the content of the depth of 0 nm, 5 nm, 10 nm and 15 nm.

Table S2. The composition of metal ions in simulated liquid low-level waste.

Metal ion	Concentration (ppm)
Na^{+}	92,300
K^{+}	19,000
Ca^{2+}	1,800
Mg^{2+}	300
Sr^{2+}	20
Al^{3+}	15
Ba^{2+}	3
Cr^{3+}	3
Pb^{2+}	3

Table S3. The contents of different functional groups calculated from XPS N1s spectra.

Materials	Peak	Binding energy (eV)	FWHM* (eV)	Area
CMPAO-1	C=N, C≡N	399.38	1.40	6116.92
	N-OH	399.98	1.41	4714.44
CMPAO-2	C=N, C≡N	399.42	1.37	7624.24
	N-OH	400.02	1.43	6852.85
CMPAO-3	C=N, C≡N	399.42	1.34	8263.25
	N-OH	400.02	1.48	7923.79
CMPAO-4	C=N, C≡N	399.35	1.65	2532.81
	N-OH	400.00	1.53	2466.18

*: Full width at half maximum.

Table S4. The contents of different functional groups calculated from XPS O1s spectra.

Materials	Peak	Binding energy (eV)	FWHM* (eV)	Area
CMPAO-1	COO^-	531.32	1.63	3606.27
	N-OH	532.65	1.88	12478.76
CMPAO-2	COO^-	531.46	1.84	5175.92
	N-OH	532.71	1.93	16828.33
CMPAO-3	COO^-	531.50	1.83	6057.20
	N-OH	532.75	1.84	15545.02
CMPAO-4	COO^-	531.32	1.87	5254.79
	N-OH	532.60	1.97	10541.46

*: Full width at half maximum.

Table S5. Elemental analysis of CMPCN and CMPAO-1~4.

Sorbent	N (%)	C (%)	H (%)
CMPCN	5.511	79.26	4.150
CMPAO-1	8.453	70.10	5.361
CMPAO-2	8.849	68.27	5.644
CMPAO-3	9.527	67.73	5.764
CMPAO-4	8.204	64.42	5.69

Table S6. Multi-Point BET parameters for CMPH, CMPCN and CMPAO-1~4.

Sorbent	V_m (cc/g)	C	R^2
CMPTF	0.137	1046.003	1.000
CMPCN	20.455	-57.481	0.999
CMPAO-1	0.021	6.223	0.999
CMPAO-2	0.010	8.447	0.996
CMPAO-3	0.011	16.731	1.000
CMPAO-4	0.013	51.551	0.999

Table S7. Kinetic parameters for the sorption of U(VI) by CMPAO-1~4. (Experimental conditions: C_{CMPAO} = 0.25 mg/mL, $C_{U\ (VI)}$ = 5×10^{-5} mol/L, pH 6.0±0.1, 298.15 K)

Sorbent	$q_{e,exp}$ (mg/g)	Pseudo-first-order			Pseudo-second-order		
		k_1 (min^{-1})	$q_{e,cal}$ (mg/g)	R^2	k_2 (g/min/mg)	$q_{e,cal}$ (mg/g)	R^2
CMPAO-1	31.513	0.0026	24.099	0.962	2.639E-4	33.921	0.995
CMPAO-2	22.774	0.0032	15.983	0.948	8.156E-5	23.041	0.993
CMPAO-3	23.642	0.0016	20.292	0.858	6.500E-4	24.882	0.997
CMPAO-4	45.789	0.0039	27.899	0.900	3.987E-4	46.926	0.997

Table S8. Langmuir and Freundlich parameters for the sorption of U(VI) by CMPAO-1~4. (Experimental conditions: C_{CMPAO} = 0.25 mg/mL, $C_{U\ (VI)}$ = 5×10^{-5} mol/L, pH 6.0±0.1, 298.15 K)

Sorbent	Langmuir			Freundlich		
	q_{max} (mg/g)	b (L/mg)	R^2	K_F (L/g)	n	R^2
CMPAO-1	156.5	0.0316	0.998	13.493	2.089	0.941
CMPAO-2	147.7	0.0167	0.996	6.162	1.693	0.961
CMPAO-3	149.0	0.0167	0.998	4.876	1.538	0.964
CMPAO-4	251.9	0.1099	0.997	47.543	2.662	0.962

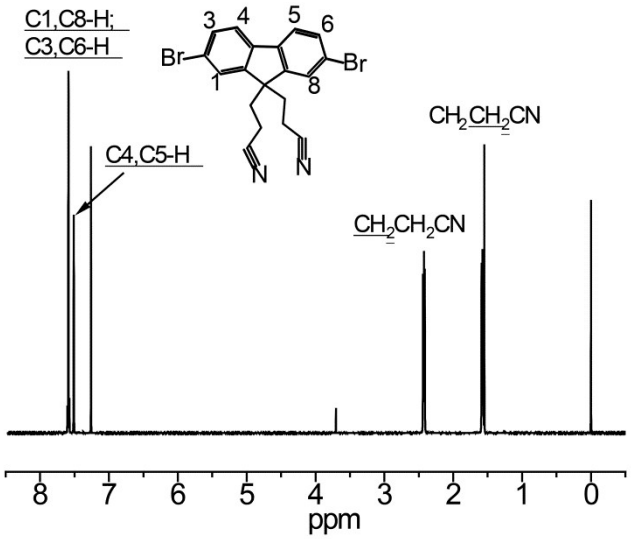

Figure S1. ^{1}H NMR spectrum of FCN

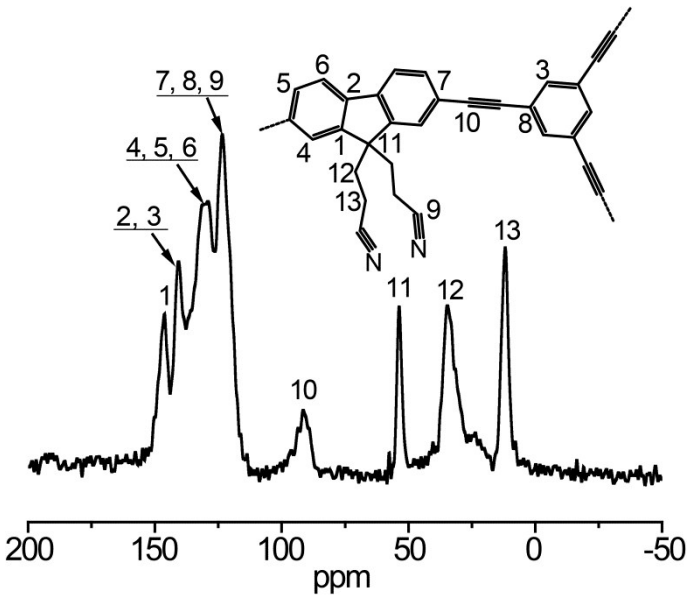

Figure S2. Solid-state ^{13}C NMR spectrum of CMPCN.

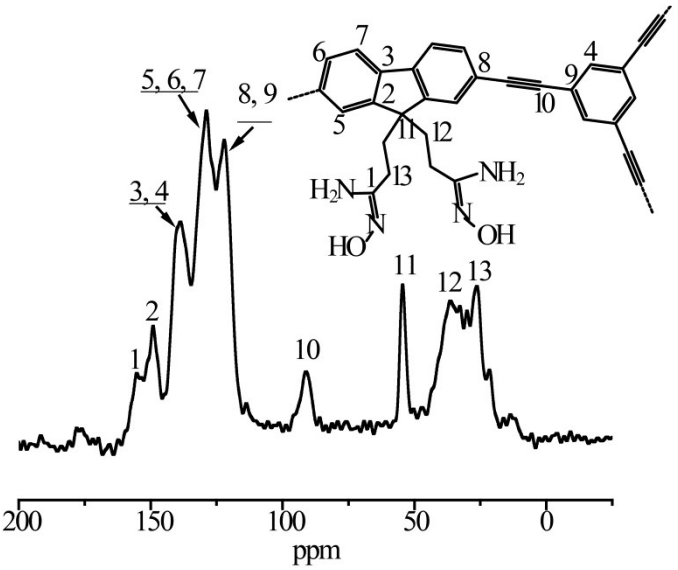

Figure S3. Solid-state ^{13}C NMR spectrum of CMPAO-2.

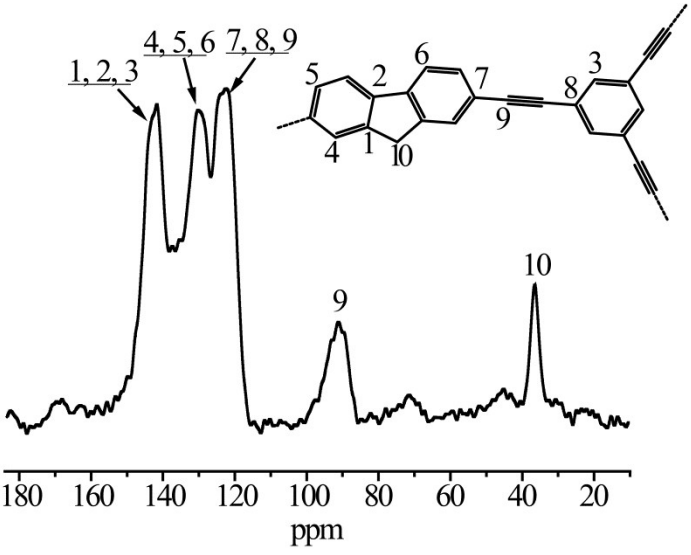

Figure S4. Solid-state ^{13}C NMR spectrum of CMPH

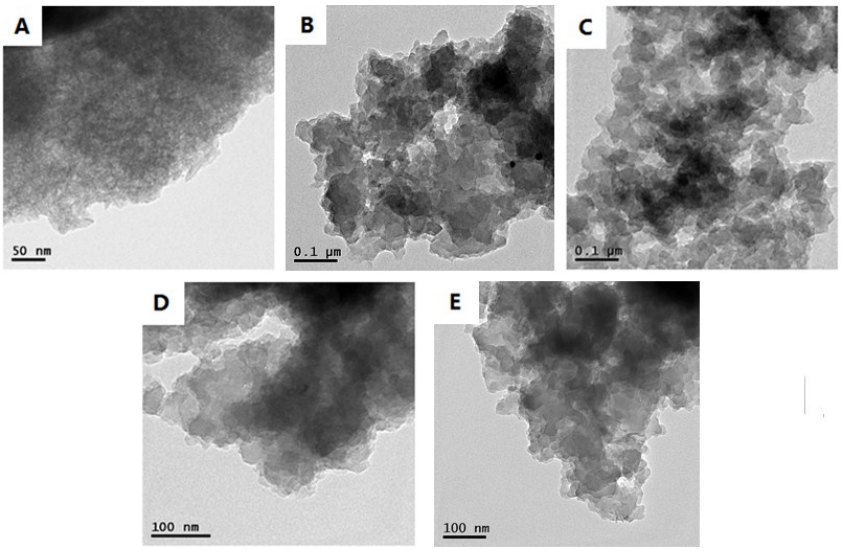

Figure S5. TEM images of (A) CMPCN, (B) CMPAO-1, (C) CMPAO-2, (D) CMPAO-3, (E) CMPAO-4

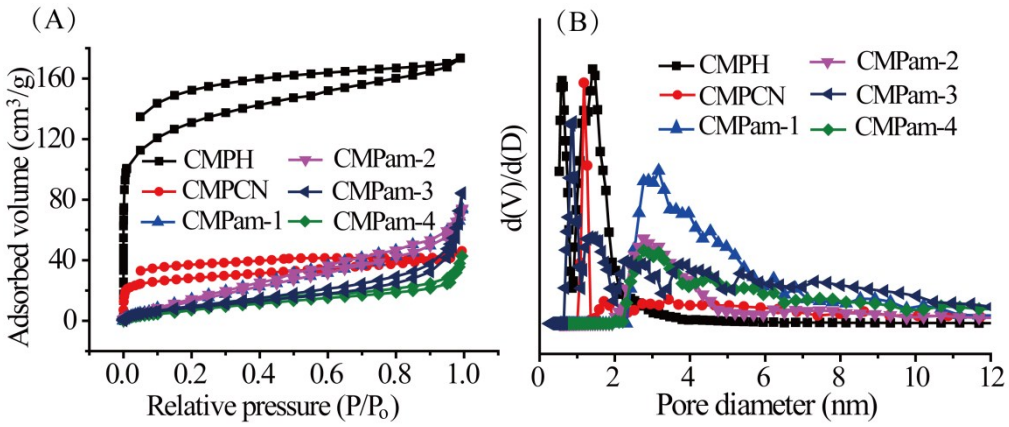

Figure S6. (A) Nitrogen sorption/desorption isotherms and (B) pore size distribution for CMPH, CMPCN and CMPAO-1~4.

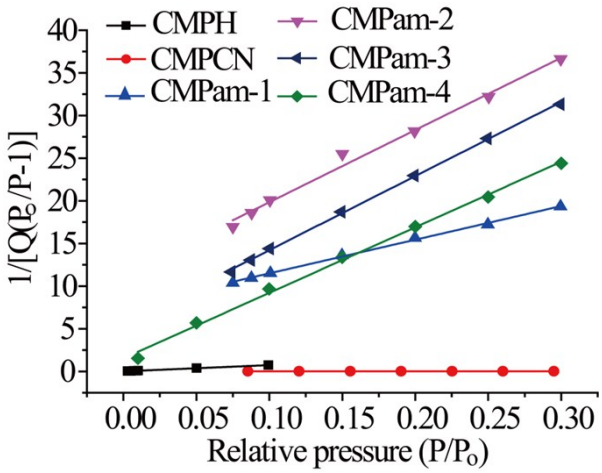

Figure S7. BET Surface Area Plot of CMPH, CMPCN and CMPAO.

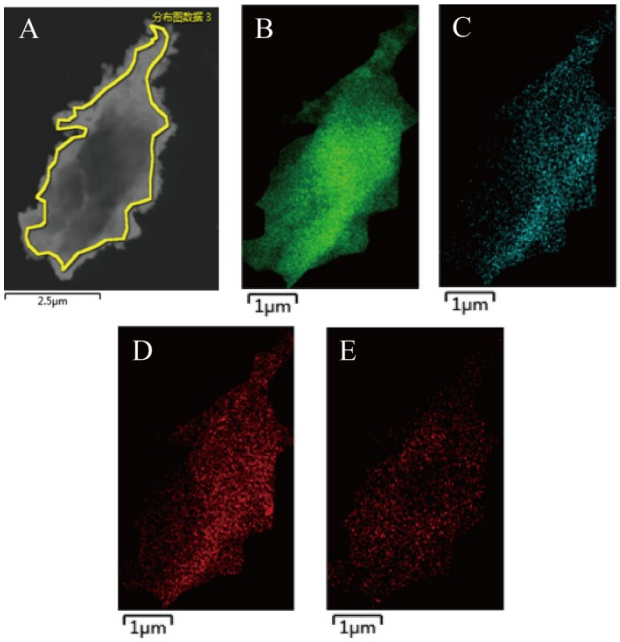

Figure S8. (A) HAADF-STEM image, (B) carbon, (C) nitrogen, (D) oxygen, and (E) uranium elemental mapping of the CMPAO-U(VI).

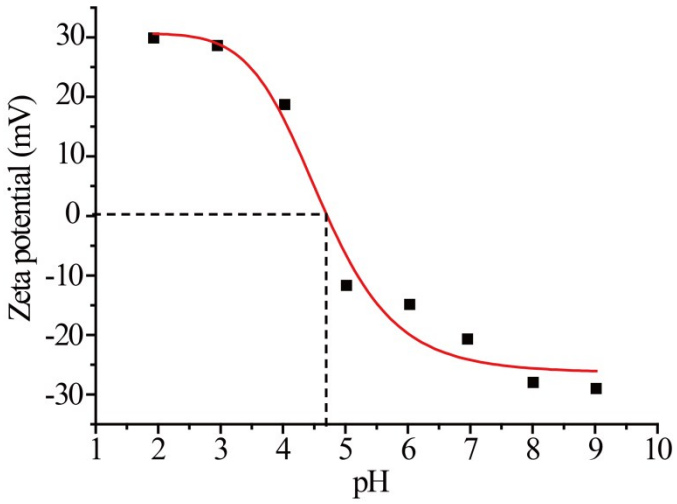

Figure S9. Zeta potential of CMPAO-4.

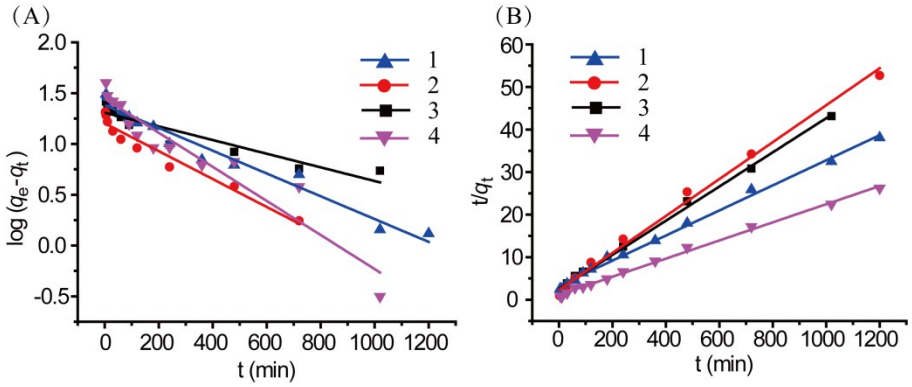

Figure S10. Kinetic models for the sorption of U(VI) onto the CMPAO-1~4. (A) Pseudo-first order model and (B) pseudo-second order.

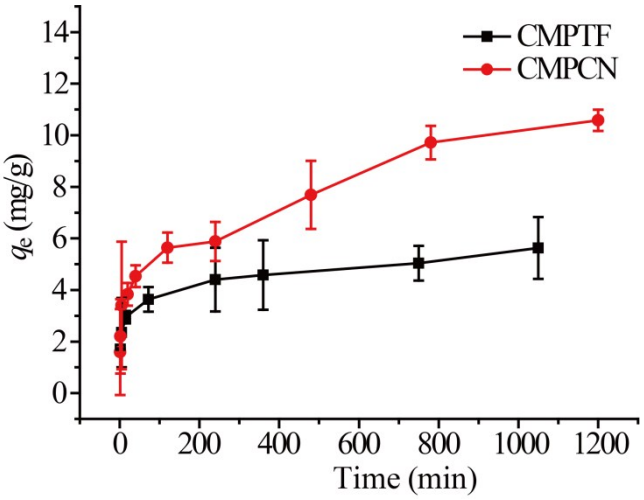

Figure S11. (A) Sorption kinetics of CMPTF and CMPCN for U(VI) (Experimental conditions: $C_{sorbent}$ = 0.25 mg mL^{-1}, $C_{U\ (VI)}$ = 5×10^{-5} mol L^{-1}, pH 6.0±0.1, and 298.15 K).

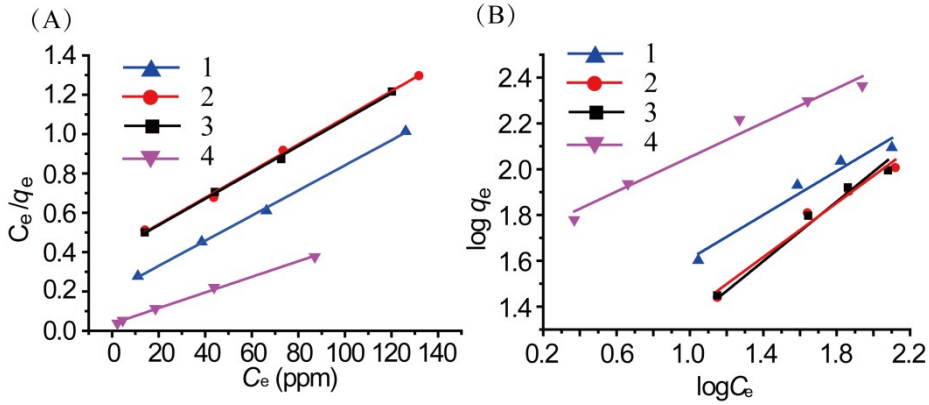

Figure S12. (A) Langmuir isotherm model and (B) Freundlich isotherm model for the sorption of U(VI) onto the CMPAO-1~4.

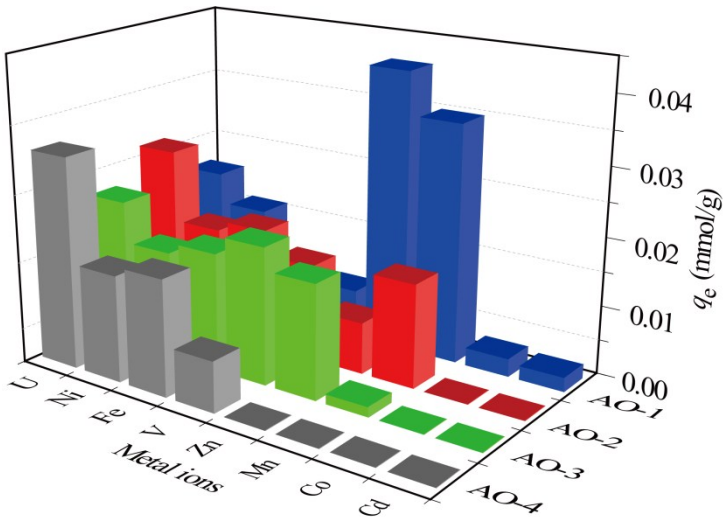

Figure S13. The sorption capacity for U (VI) and competing metal ions on CMPAO-1~4 in seawater with additional ions. (Experimental conditions: $C_{sorbent}$ = 0.25 mg mL^{-1}, $C_{metal\ ions}$ = 2×10^{-5} M, and 298.15 K).

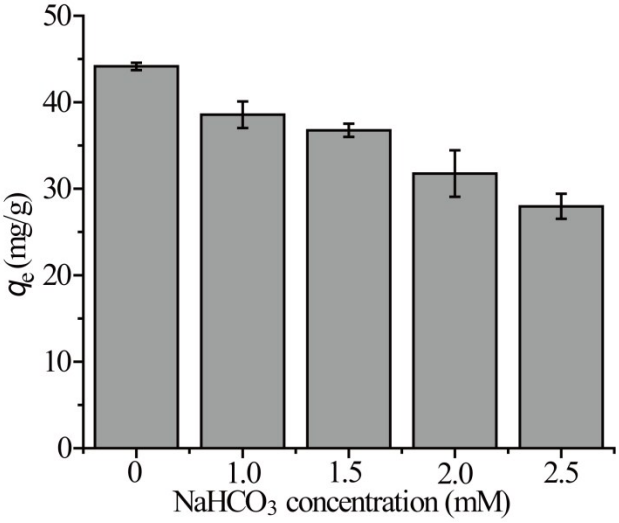

Figure S14. The effect of salt concentration on sorption and reusability of CMPAO. (A) The effect of salt concentration on sorption; (B) reusability (Experimental conditions: $C_{sorbent}$ = 0.25 mg mL^{-1}, C_U = 5×10^{-5} M, and 298.15 K).

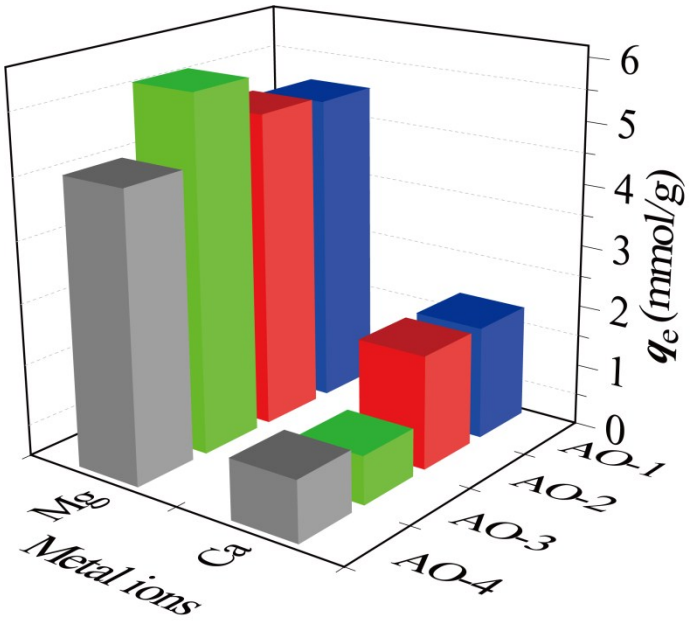

Figure S15. The sorption capacity for Ca^{2+} and Mg^{2+} on CMPAO-1~4 in seawater with additional ions. (Experimental conditions: $C_{sorbent}$ = 0.25 mg mL^{-1}, $C_{metal\ ions}$ = 2×10^{-5} M, 298.15 K).

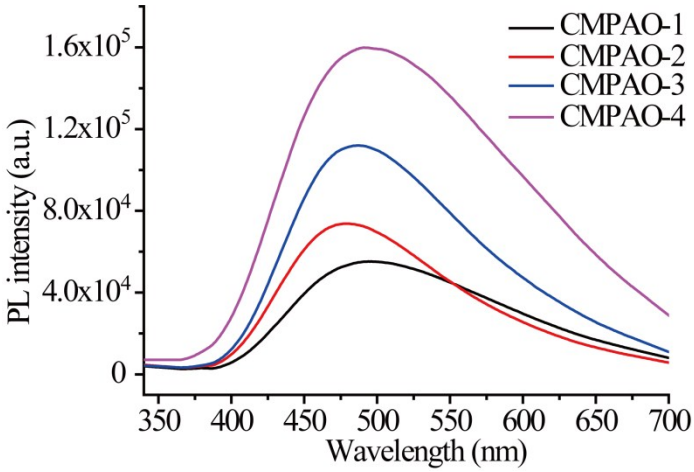

Figure S16. Emission spectra of CMPAO-4 in uranyl solution (λ_{ex} = 320 nm, $C_{sorbent}$ = 0.20 mg mL^{-1}, T = 298.15 K).

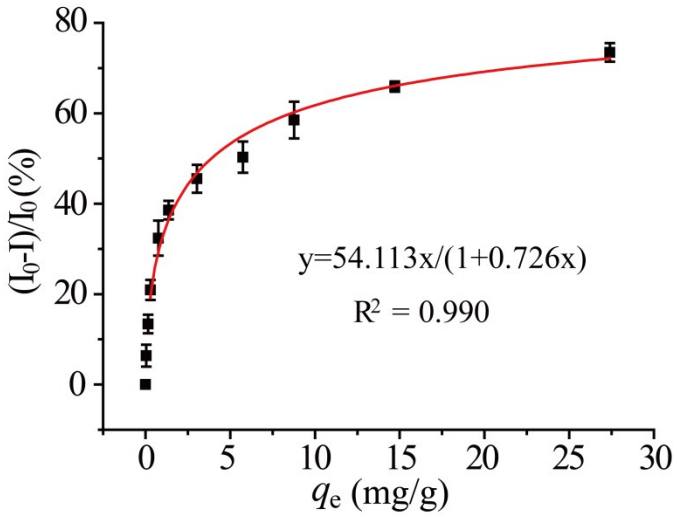

Figure S17. Correlation between the quenching factor and sorption capacity of CMPAO-4 (λ_{ex} = 320 nm, data at 483 nm was selected for analysis. $C_{sorbent}$ = 0.20 mg mL^{-1}, T = 298.15 K).

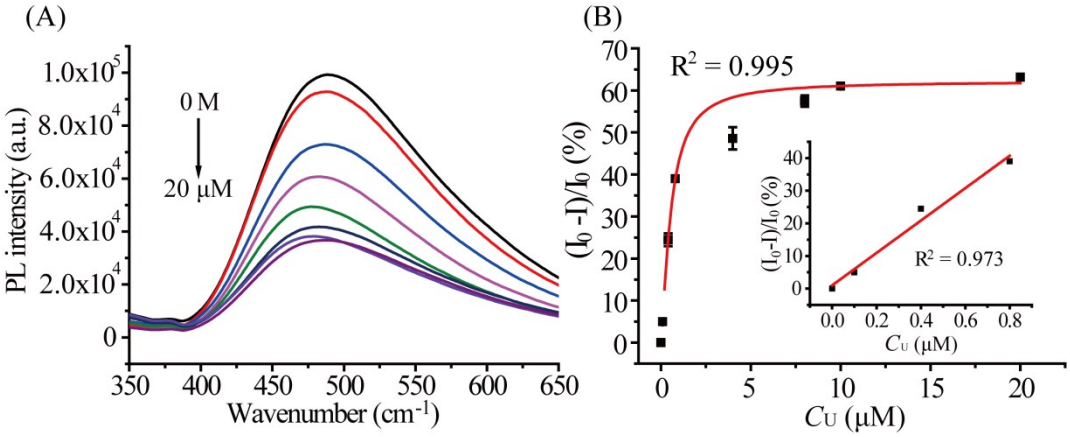

Figure S18. Fluorescence-based uranyl detection studies. (A) Emission spectra of CMPAO-4 in simulated liquid low-level waste with varying uranyl concentration (0~20 μM). (B) Simulated correlation between quenching ratio [(I_0−I)/I_0]% and UO_2^{2+} concentration using the Langmuir model. The inset is the relative decrease of luminescence intensity (measured at 483 nm) of CMPAO-4 as a function of the uranyl concentration in low concentration (0-0.8 μM) (λ_{ex} = 320 nm, data at 483 nm was selected for analysis. $C_{sorbent}$ = 0.20 mg mL^{-1}, T = 298.15 K).

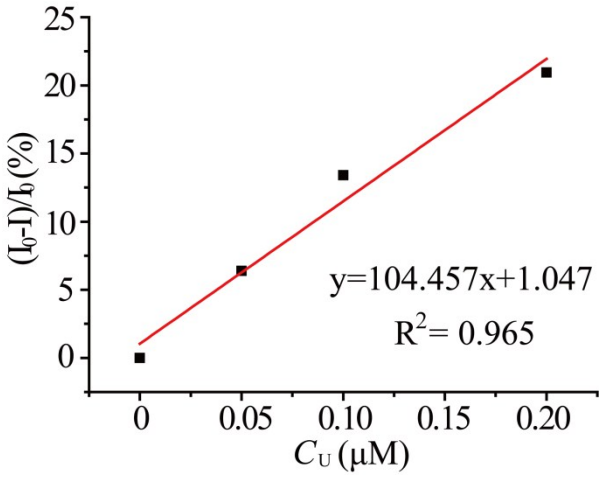

Figure S19. The relative decrease of luminescence intensity (measured at 483 nm) of CMPAO-4 as a function of the uranyl concentration in low concentration (0-0.2 μM) are fitted in linear relationship (λ_{ex} = 320 nm, data at 483 nm was selected for analysis. $C_{sorbent}$ = 0.20 mg mL^{-1}, T = 298.15 K).

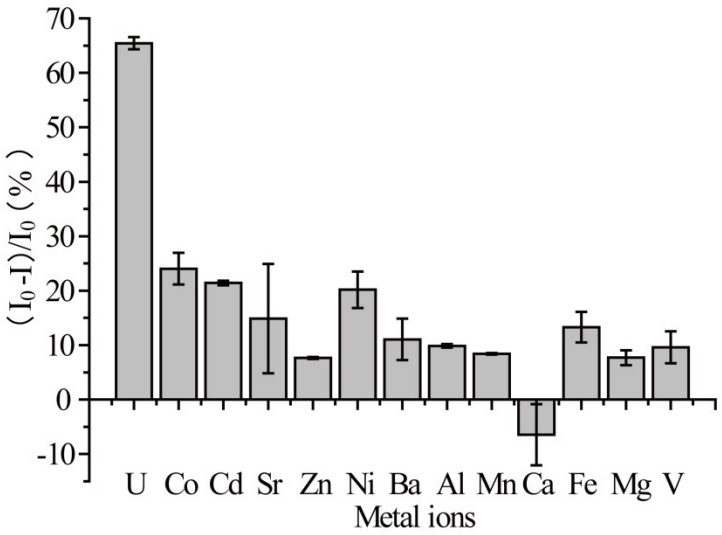

Figure S20. Luminescence quenching ratio of CMPAO-1~4 in different metal salt solutions (λ_{ex} = 320 nm, data at 483 nm was selected for analysis. $C_{sorbent}$ = 0.20 mg mL^{-1}, T = 298.15 K).

References

1. Han X, Xu M, Yang S, Qian J, Hua D. Acetylcysteine-functionalized microporous conjugated polymers for potential separation of uranium from radioactive effluents. *Journal of Materials Chemistry A* **5**, 5123-5128 (2017).
2. Kiskan B, Weber J. Versatile Postmodification of Conjugated Microporous Polymers Using Thiol-yne Chemistry. *ACS Macro Letter* **1**, 37–40 (2012).
3. Ho YS, McKay G. Pseudo-second order model for sorption processes. *Process Biochemistry* **34**, 451-465 (1999).
4. Ho YS, McKay G. The kinetics of sorption of divalent metal ions onto sphagnum moss peat. *Water Research* **34**, 735-742 (2000).
5. Sadeghi S, Aboobakri E. Magnetic nanoparticles with an imprinted polymer coating for the selective extraction of uranyl ions. *Microchimica Acta* **178**, 89-97 (2012).
6. Zhang S*, et al.* "Stereoscopic" 2D super-microporous phosphazene-based covalent organic framework: Design, synthesis and selective sorption towards uranium at high acidic condition. *Journal of Hazardous Materials* **314**, 95-104 (2016).
7. Liu W*, et al.* Highly Sensitive and Selective Uranium Detection in Natural Water Systems Using a Luminescent Mesoporous Metal-Organic Framework Equipped with Abundant Lewis Basic Sites: A Combined Batch, X-ray Absorption Spectroscopy, and First Principles Simulation Investigation. *Environ Sci Technol* **51**, 3911-3921 (2017).